J. Min. Metall. Sect. B-Metall. 55 (2) B (2019) 197 - 208

Journal of Mining and Metallurgy, Section B: Metallurgy

CHLORINE CORROSION OF BLAST FURNACE GAS PIPELINES: ANALYSIS FROM THERMAL PERSPECTIVE

W.-Q. Sun [a,b,c*], X.-D. Xu [b], Y. Zhang [d], J.-Z. Wu [b]

[a] Department of Thermal Engineering, School of Metallurgy, Northeastern University, Shenyang, Liaoning, China

[b] School of Engineering, Cardiff University, Wales, United Kingdom

[c] State Environmental Protection Key Laboratory of Eco-Industry, Shenyang, Liaoning, China

[d] R&D Centre, Hisense Group Co., Ltd., Qingdao, Shandong, China

(Received 16 October 2018; accepted 25 April 2019)

Abstract

With the broad application of dry dedusting of blast furnace gas (BFG), the issue of BFG pipeline corrosion comes up because of chlorine in the BFG. Existing methods in preventing the corrosion, such as spraying alkali or installing corrosion-resistant materials, require a significant amount of investment. This paper conducted a novel thermal analysis of the corrosion mechanism to support the study on corrosion prevention without using additional materials. Firstly, thermal models were established to reflect the relationships among the amount of condensation water, the mass transfer rate, the concentration of chloride ion and the ambient temperature. Secondly, the relationship between BFG temperature and the corrosion rate was obtained via a cyclic exposure experiment. Key factors that affect the pipeline corrosion under various BFG temperatures were identified. Finally, a control scheme of the BFG temperature was proposed to avoid the chlorine corrosion.

***Keywords**: Chlorine corrosion; Blast furnace gas pipeline; Dry dedusting; Thermal analysis; Cyclic exposure test.*

1. Introduction

Blast furnace gas (BFG) is a by-product of ironmaking processes. One tonne of the pig iron yields approximately 1700 m^3 of BFG. Meanwhile, BFG is also an important secondary energy source with the heating value of 3000 to 4000 kJ/m^3. In the steel industry, BFG are transported among different plants through pipeline networks [1]. In most steel sites, the pipeline network of BFG is the largest energy transport network [2]. Yet, more and more accidental shutdowns occur in recent years due to the corrosion of BFG pipelines and the blade vibration of top pressure recovery turbines (TRT) [3]. These shutdowns seriously influence the safety of blast furnaces and may be propagated to the whole steel plants. This phenomenon has been intensively studied [4], but the problem is still not solved.

As the dust in raw BFG may lead to the blocking and abrasion of pipelines, burners and valves, a dedusting process is usually conducted before injecting the BFG into the pipeline network [5,6]. Wet dedusting is a traditional technology used in the ironmaking process but has critical defects, such as colossal water consumption and the resultant sewage, significant temperature and pressure drops of BFG and the resultant energy loss, and high contents of saturated moisture and mechanical moisture. As a result, the dry dedusting technology was developed to avoid these defects. Since no spraying water is needed, this technology saves 0.7 to 0.9 m^3 water for the production of pig iron per tonne. The sensible heat and pressure of BFG is also extracted to drive dry TRT. Thus, the dry TRT generates 30% electricity more than the wet TRT [6]. Accordingly, dry TRT was listed as a promising energy-saving technology together with other waste energy recovery technologies [7,8]. Unfortunately, the corrosives in dry dedusting BFG destroy the BFG pipelines and consumers seriously, and bring a critical threat to the BFG system. The rapid and severe corrosion issue, which has not been encountered in the wet dedusting process, has become an industrial conundrum.

The corrosion of steel has been studied previously [9,10]. The types of BFG pipelines corrosion include pitting corrosion, stress corrosion, and erosion

**Corresponding author: sunwq@mail.neu.edu.cn*

DOI:10.2298/JMMB181016028S

corrosion. Five factors may affect the corrosion rate of BFG pipelines, namely physical properties of BFG (moisture, temperature, pressure, and flow rate), features of BFG condensation water (pH and chloride ion content), ambient conditions (ambient temperature, moisture, and wind velocity), characteristics of pipelines (material and thickness) and the corrosion product film. Localised corrosion with very high corrosion rates usually occurs when the corrosion product film does not provide sufficient protection. This is the most serious corrosion in BFG pipelines [11].

According to [12,13], the corrosion of BFG pipelines is mainly caused by chlorine. Three kinds of chloride exist in the BFG, including HCl, NH_4Cl and NaCl (or KCl, ZnCl, etc.) [2]. Geerdes et al. [14] pointed out that the chlorine content caused corrosion of the steel in the BFG cleaning system. To grasp the chlorine contributor, Hu et al. [15] conducted a chlorine element balance of a blast furnace at Tangsteel, China. It was observed that coke and pulverised coal were the main sources of chlorine. Removing chlorine dominated the cost of cleaning BFG. Murav'eva and Bebeshko [16] and Bartusch et al. [17] carried out mass balance and equilibrium calculations at Hüttenwerke Krupp Mannesmann. It was reported that chloride in the BFG led to the corrosion of pipelines, hot stoves, air heaters, and tuyeres of the blast furnace. Hu et al. [18] found that the chlorine entering the blast furnace merged with BFG in the form of HCl after a series of chemical reactions. The corrosions of gas pipelines and TRT blades are aggravated by the chloride ion in the BFG condensation water, which also affects the conveying process of BFG and the operation of the TRT unit. To alleviate the negative influence of the problem, technologies, such as gas dechlorination [2], TRT antiscale, spraying lime powder [20], use of low chloride additives [20] in the sintering process, and corrosion-resistant alloys [11], were developed for BFG transport.

Since the BFG pipelines corrosion mainly results from the chloride ion, it is necessary to identify the factors influencing the chloride ion content in the condensation water. Most literature focuses on the use of anti-corrosion materials [21] and the reduction of chlorinated iron ores, whereas few investigations were conducted from the thermal perspective [22]. This paper aims to analyse the form of corrosive condensation water and the content of the chloride ion from the following aspects: 1) The amount of condensation water at different ambient temperatures and dew points of BFG; 2) The mass transfer and the diffusion rate of the chloride ion. The relationship of BFG pipelines corrosion rate and the temperature of BFG is investigated by proceeding a cycle infiltration corrosion-accelerating experiment. Based on the relationship, an anticorrosion scheme is proposed, by using the process heat from the blast furnace instead of changing the material of pipelines.

2. Thermal Models

Because no water spraying is used, the temperature of cleaned BFG after dry dedusting is still higher than the dew point. Thus, at the initial stage, it is difficult to separate the condensation water and the concomitant chloride ion from the BFG. If the BFG flows through a pressure reducing valves unit or a TRT unit, the pressure and temperature of the BFG will reduce significantly, at which time the condensation water and crystals emerge. The temperature of the BFG reduces progressively along the conveying process of the BFG. Thus, a large amount of condensation water is precipitated, in which the chloride ion is dissolved to be a highly acid and corrosive solution. This corrosion occurs only if the temperature of the BFG is lower than its dew point temperature, which is also relative to the temperature and moisture content of the BFG and the ambient temperature. To understand the mechanism of condensation heat transfer, mass transfer heat transfer, and thermodynamics analysis are modelled. The relationship between the temperature drop of BFG and condensation water amount and chloride ion content is reflected through the models.

2.1 Condensation Water Calculation Model

The temperature of the BFG decreases along the transport pipelines because of its heat exchange with the surroundings. The moisture begins to be condensed when the temperature of the BFG reaches its dew point temperature. The more significant the temperature drop, the more the amount of condensation water. The BFG is considered as an ideal gas, then the moisture content in real BFG is defined as the mass of H_2O per unit volume of dry BFG, which is calculated from

$$a = \frac{m_{H_2O}}{V_{BFG}} = \frac{M_{H_2O} \cdot n_{H_2O}}{V_{mBFG} \cdot n_{BFG}} \tag{1}$$

where a is the moisture content of dry BFG [g(H_2O)/Nm^3(dry BFG)]; m_{H_2O} is the mass of water [g]; V_{BFG} is the volume of dry BFG [Nm^3]; M_{H_2O} is the molar mass of water [g/mol]; V_{mBFG} is the molar volume of dry BFG [Nm^3/mol]; n_{H_2O} and n_{BFG} are the amount of substance [mol] for water and dry BFG, respectively.

Given that the ratio of the amount of substance of each component in the BFG is equal to the ratio of the partial pressure of each component, and, $p' = p - p_v$ then Eq. (1) can be rewritten as

$$a = \frac{M_{H_2O}}{V_{mBFG}} \cdot \frac{p_v}{p - p_v} \tag{2}$$

where p and p_v are the partial pressures [Pa] of dry

BFG and H_2O at temperature t [K], respectively; and p is the pressure of real BFG [Pa].

According to the ideal gas law, for saturated BFG, the molar volume and partial pressure of water are as follows:

$$V^*_{m\mathrm{BFG}} = \frac{p \cdot V_{m\mathrm{BFG}}}{T} \cdot \frac{T^*}{p^*} \tag{3}$$

$$p^*_v = \frac{p^* \cdot a \cdot V^*_{m\mathrm{BFG}}}{M_{\mathrm{H_2O}} + a \cdot V^*_{m\mathrm{BFG}}} \tag{4}$$

where T is the absolute temperature of the BFG [K]; and the superscript * represents the saturated state. The dew point temperature (T_a) is obtained by referring to the thermodynamic properties of vapour.

Thus, the amount of condensation water (Q) is

$$Q = Q(T_a) - Q(T) \tag{5}$$

where $Q(T_a)$ is the saturated moisture content of the BFG at the dew point temperature [kg/h]; $Q(T)$ is the saturated moisture content of the BFG at temperature T which is lower than T_a.

2.2 Heat Transfer Model

The water condensation of the BFG in a horizontal pipeline is schematically shown in Fig. 1. As shown in Fig. 1(a), the BFG enters the pipelines at point 1, reaches its saturation point at point 2 where the condensation begins to happen. Because the moving velocity of the BFG is higher than the condensation water, the flow pattern of condensation water is annular flow. With the increasing amount of condensation water, the annular flow turns to stratified flow at point 3. At point 4, the condensation process is completed and reaches a new thermodynamic balance state. The condensation water mainly accumulates at the bottom of the pipeline, while the BFG flow mainly accumulates at the upper part of the pipeline. The section shape of the pipeline is shown in Fig. 1(b).

(1) Single-phase heat transfer coefficient inside the BFG pipelines

The forced convective heat transfer in the pipelines is described in the form of Dittus-Boelter correlation [23]:

$$Nu = 0.023 Re^{0.8} Pr^m \tag{6}$$

where m = 0.4 when the fluid is heated, while m = 0.3 when the fluid is cooled; Nu, Re and Pr are Nusselt number, Reynolds number and Prandtl number, respectively.

The single-phase heat transfer coefficient of the BFG inside the pipelines can be written as

$$h_1 = 0.023 Re^{0.8} Pr^m \cdot \frac{\lambda}{d} \tag{7}$$

where λ is the thermal conductivity of the BFG [W/(m·K)]; d is the internal diameter of the pipeline [m].

(2) Condensation heat transfer coefficient inside the BFG pipelines

Several convective heat transfer models have been developed by researchers [24]. Given the shearing force of the BFG is relatively small, according to Chaddock [25] and Chato [26], the circular average heat transfer film coefficient inside the BFG pipelines is

$$h'_1 = 0.555 \cdot \left[\frac{\lambda_L^3 \rho_L (\rho_L - \rho) g \left(r + 3c_p (t - t_w)/8\right)}{\mu_L d (t - t_w)} \right]^{1/4} \tag{8}$$

where λ_L is the thermal conductivity of condensation water [W/(m·K)]; ρ and ρ_L are the densities of BFG and condensation water, respectively [kg/m^3]; r is the latent heat of BFG condensation [kJ/kg]; c_p is the specific heat at constant pressure of condensation water [kJ/(kg·K)]; t_w is the wall temperature of pipelines [K]; g is the acceleration of gravity [m/s^2]; and μ_L is the viscosity of the condensation water [N·s/m^2].

(3) Heat transfer coefficient outside BFG pipelines

The heat transfer between BFG pipelines and the surroundings is similar to natural convection in a large space, with correlation formulas in [27]

$$Nu_m = C (Gr \cdot Pr)^n_m \tag{9}$$

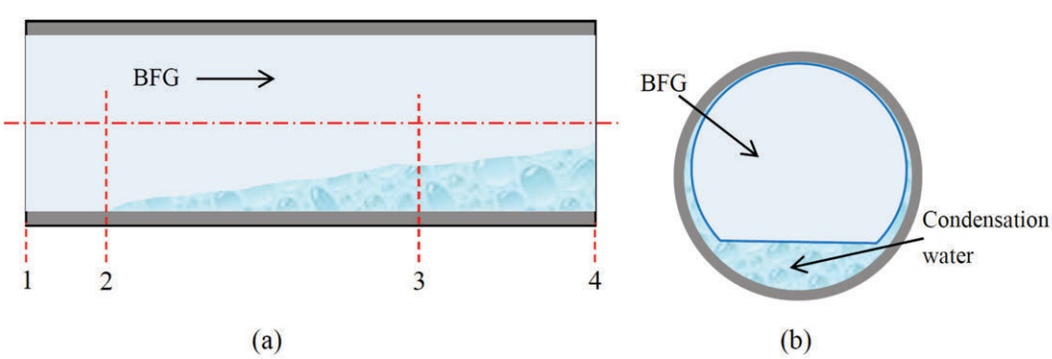

Figure 1. *The schematic diagram of moisture separation from the BFG: (a) Condensation process in a horizontal BFG pipeline; (b) Sectional view of a BFG pipeline*

and $Gr = \dfrac{g\alpha_V (t_w - t_\infty) d^3}{v^2}$ (10)

where the subscript m represents the mean temperature [K]; t_∞ is the ambient temperature [K]; α_V is the coefficient of cubic expansion with the value of $1/T$; and C and n are constants as listed in Table 1, respectively.

According to Eqs. (9) and (10) and Table 1, the heat transfer coefficient outside BFG pipelines is expressed as:

$$h_2 = C\left(\frac{g\alpha_V (t_w - t_\infty) d^3}{v^2} \cdot Pr\right)_m^n \cdot \frac{\lambda}{d} \quad (11)$$

(4) Thermal resistance of the wall of BFG pipelines

BFG pipelines are covered by a thermal insulator and a protective layer, so the heat transfer through the BFG pipelines is regarded as the heat transfer through a three-layer cylindrical wall, as shown in Fig. 2. The internal diameter of the pipeline wall is d_1 with the temperature of the inner wall as t_1. The external diameter of the pipeline wall is d_2 with the temperature of the outer wall as t_2. The external diameter of the thermal insulator is d_3 with the temperature of the interface of thermal insulator and protective layer as t_3. The external diameter of the protective layer is d_4 with the temperature of the outer surface of the protective layer as t_4, and l is the investigated length of the BFG pipeline.

Each layer is considered as a uniform material with the thermal conductivities of λ_1, λ_2 and λ_3, respectively. Then, the total thermal resistance of the three-layer cylindrical walls is

$$R = \frac{\frac{1}{\lambda_1}\ln\frac{d_2}{d_1} + \frac{1}{\lambda_2}\ln\frac{d_3}{d_2} + \frac{1}{\lambda_3}\ln\frac{d_4}{d_3}}{2\pi l} \quad (12)$$

(5) Heat transfer of the BFG pipelines

(a) for single-phase heat transfer section

The convective heat transfer from the BFG to the inner wall of the pipelines is

$$\varphi_1 = h_1 \cdot \pi \cdot d_1 \cdot l_1 \cdot (T - t_1) \quad (13)$$

where l_1 is the length of the single-phase section [m], T and t_1 are the mean temperature of BFG and the inner wall of the single-phase section [K], respectively.

The conductive heat transfer through the three-layer cylindrical walls is

$$\varphi_2 = \frac{2\pi l_1 (t_1 - t_4)}{\frac{1}{\lambda_1}\ln\frac{d_2}{d_1} + \frac{1}{\lambda_2}\ln\frac{d_3}{d_2} + \frac{1}{\lambda_3}\ln\frac{d_4}{d_3}} \quad (14)$$

The convective heat transfer from the outer of the pipelines to the surroundings is

$$\varphi_3 = h_2 \cdot \pi \cdot d_4 \cdot l_1 \cdot (t_4 - t) \quad (15)$$

For simplicity, the whole heat transfer process is considered as a steady-state process, then

$$\varphi_1 = \varphi_2 = \varphi_3 = \varphi \quad (16)$$

From Eqs. (13) to (16), the heat transfer is written as

$$\varphi = \frac{\pi l_1 (T - t)}{\frac{1}{d_1 h_1} + \frac{1}{2\lambda_1}\ln\frac{d_2}{d_1} + \frac{1}{2\lambda_2}\ln\frac{d_3}{d_2} + \frac{1}{2\lambda_3}\ln\frac{d_4}{d_3} + \frac{1}{d_4 h_2}} \quad (17)$$

(b) for condensation heat transfer section

The convective heat transfer from the BFG to the inner wall of the pipeline is

$$\varphi_1' = h_1' \cdot \pi \cdot d_1 \cdot l_2 \cdot (T' - t_1') \quad (18)$$

where l_1 is the length of the condensation section [m], and the superscript ′ represents the parameter at the condensation heat transfer section.

Table 1. *The constant coefficients of C and n of Eq. (9)*

Flow pattern	C	n	scope of application
Laminar flow	0.48	1/4	$1.43\times10^4 \le Gr < 5.76\times10^8$
Transition flow	0.0165	0.42	$5.76\times10^8 \le Gr < 4.65\times10^9$
Turbulent flow	0.11	1/3	$Gr > 4.65\times10^9$

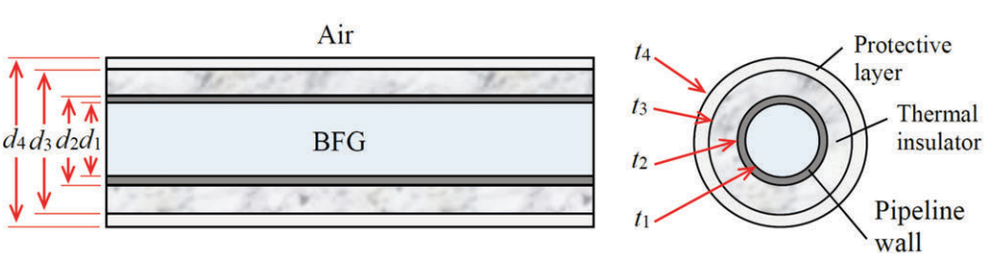

Figure 2. *The schematic structure of BFG pipelines*

The conductive heat transfer through the three-layer cylindrical walls is

$$\varphi_2' = \frac{2\pi l_2 \left(t_1' - t_4'\right)}{\frac{1}{\lambda_1}\ln\frac{d_2}{d_1} + \frac{1}{\lambda_2}\ln\frac{d_3}{d_2} + \frac{1}{\lambda_3}\ln\frac{d_4}{d_3}} \tag{19}$$

The convective heat transfer from the outer of the pipelines to the surroundings is

$$\varphi_3' = h_2' \cdot \pi \cdot d_4 \cdot l_2 \cdot \left(t_4' - t\right) \tag{20}$$

Also,

$$\varphi_1' = \varphi_2' = \varphi_3' = \varphi' \tag{21}$$

From Eqs. (18) to (21), the heat transfer is written as

$$\varphi' = \frac{\pi l_2 \left(T' - t\right)}{\frac{1}{d_1 h_1'} + \frac{1}{2\lambda_1}\ln\frac{d_2}{d_1} + \frac{1}{2\lambda_2}\ln\frac{d_3}{d_2} + \frac{1}{2\lambda_3}\ln\frac{d_4}{d_3} + \frac{1}{d_4 h_2'}} \tag{22}$$

Eqs. (13) to (22) are subjected to

$$l = l_1 + l_2 \tag{23}$$

(6) The temperature of the BFG at the outlet of the pipeline

Given that the temperature difference between T_1 and T_a is small (around 10 K in this application) during the single-phase convection process, the change in the BFG density is neglected. According to the energy balance, the heat released by the BFG during the single-phase convection process is expressed as

$$q = \rho \cdot u \cdot \frac{\pi d_1^2}{4} \cdot c_p \cdot \left(T_1 - T_a\right) \tag{24}$$

where u is the velocity of the BFG [m/s], and T_1 is the temperature of the BFG at the inlet of the pipelines [K].

The heat released by the BFG during the condensation convention process is

$$q' = \rho \cdot u \cdot \frac{\pi d_1^2}{4} \cdot c_p \cdot \left(T_a - T_2\right) \tag{25}$$

where T_2 is the temperature of BFG at the outlet of the pipelines [K].

It is evident that $q = \varphi$ and $q' = \varphi'$. Thus, the length of the single-phase convection section is

$$l_1 = \rho u \frac{\pi d_1^2}{4} c_p \left(T_1 - T_a\right) \cdot \frac{\frac{1}{d_1 h_1} + \frac{1}{2\lambda_1}\ln\frac{d_2}{d_1} + \frac{1}{2\lambda_2}\ln\frac{d_3}{d_2} + \frac{1}{2\lambda_3}\ln\frac{d_4}{d_3} + \frac{1}{d_4 h_2}}{\pi\left(T - t\right)} \tag{26}$$

The temperature of BFG at the outlet of the pipeline is:

$$T_2 = T_a - \frac{\varphi'}{\rho u \frac{\pi d_1^2}{4} c_p} \tag{27}$$

2.3 Mass Transfer Model

To further analyse the corrosion mechanism, a mass transfer based kinetic model of diffusion corrosion is established. The model considers the gas-liquid mass transfer and the diffusion rate of chloride ion in the condensation water. Given the chloride ion is the primary driver of the corrosion of BFG pipelines, only the HCl-H_2O system is investigated in this mass transfer model. The condensed droplets are attached on the inner surface of the BFG pipelines. Chloride ions are diffused into the droplets via mass transfer, as shown in Fig. 3. The droplet is so small that the inner wall of the BFG pipeline is considered as a horizontal surface.

(1) Phase equilibrium coefficient

According to the two-film theory proposed by Whitman [28], the phase equilibrium coefficient of the ideal BFG component system is

$$m = \frac{p^0}{p} \tag{28}$$

where p^0 is the saturated vapour pressure of a pure component at the equilibrium temperature [kPa].

Assume that the saturated pressure of H_2O can be obtained from several thermodynamic parameter databases, then the saturated pressure of HCl is estimated by Riedel-Plank-Miller equation [29]:

$$\ln\frac{p^0}{p_c} = \frac{GT_c}{T}\left[1 - \left(\frac{T}{T_c}\right)^2 + k\left(3 + \frac{T}{T_c}\right)\left(1 - \frac{T}{T_c}\right)^3\right] \tag{29}$$

$$G = 0.4835 + 0.4605h \tag{30}$$

$$k = \frac{\frac{h}{G} - \left(1 + \frac{T_b}{T_c}\right)}{\left(3 + \frac{T_b}{T_c}\right)\left(1 - \frac{T_b}{T_c}\right)^2} \tag{31}$$

and

$$h = \frac{T_b \ln P_c}{T_c - T_b} \tag{32}$$

where subscripts b and c represent the boiling point and critical point, respectively. The values of T_b, T_c and p_c are 188.1 K, 324.6 K and 8309 kPa, respectively.

(2) Diffusion rates

According to the molecular kinetic theory, the gaseous phase diffusion rate is calculated by [30]

$$D_g = \frac{1.8583\times10^{-7} T^{3/2}}{p\sigma^2\Omega_D}\left(\frac{1}{M_{HCl}} + \frac{1}{M_{H_2O}}\right)^{1/2} \tag{33}$$

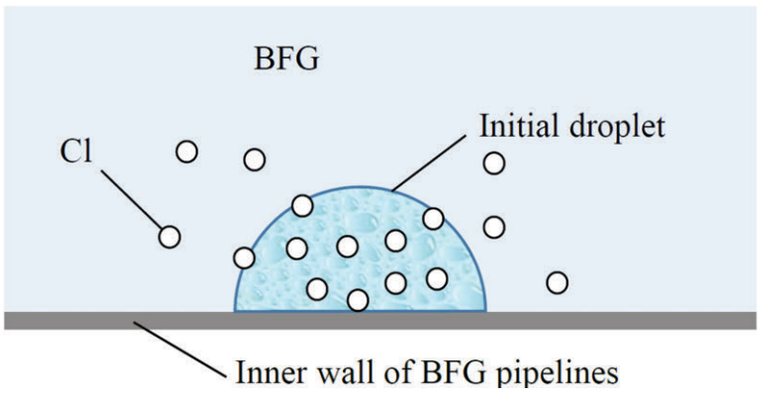

Figure 3. *The schematic diagram of the chloride ion diffusion process*

and

$$\Omega = f\left(\frac{K_B T}{\varepsilon}\right) \tag{34}$$

where σ is the collision diameter of HCl and H_2O, subjected to $\sigma=\left(\sigma_{HCl}+\sigma_{H_2O}\right)/2$ [Å]; ε is the interaction energy of HCl and H_2O, subjected to $\varepsilon=\sqrt{\varepsilon_{HCl}\cdot\varepsilon_{H_2O}}$ [erg]; Ω is the collision integral; and K_B is the Boltzmann constant with the value of 1.38×10^{-6} erg/K. According to Nernst formula [31], the liquid phase diffusion rate is

$$D_l = 8.931\times10^{-10} T\left(\frac{l_+^0 l_-^0}{l_+^0 + l_-^0}\right)\left(\frac{z_+ + z_-}{z_+ z_-}\right) \tag{35}$$

where l_+^0 and l_-^0 are the electrical conductivities of cation and anion, respectively; z_+ and z_- are the absolutes of positive and negative ion valency, respectively.

(3) Mass transfer coefficient

The mass transfer flux is written as

$$N = K_x\left(x_e - x\right) = K_y\left(y - y_e\right) = K\left(y - Mx\right) \tag{36}$$

where K_x and K_y are the overall mass transfer coefficients based on liquid or gas phase, respectively [kmol/(m^2·s)]; K is the overall mass transfer coefficients of the whole system, [kmol/(m^2·s)]; x and y are the HCl fractions in the liquid phase and gaseous phase before the mass transfer, respectively; x_e is the molar fraction of liquid phase which is in phase equilibrium with y; and y_e is the molar fraction of gaseous phase which is in phase equilibrium with x.

The coefficients satisfy the following relations [32]:

$$\frac{1}{K_x} = \frac{1}{M k_y} + \frac{1}{k_x}, \frac{1}{K_y} = \frac{1}{k_y} + \frac{M'}{k_x}, M' = \frac{y - y_e}{x_e - x} \tag{37}$$

or

$$\frac{1}{K} = \frac{1}{K_y} + \frac{M}{K_x}, M = \frac{y_e}{x_e} \tag{38}$$

where k_x and k_y are the individual mass transfer coefficients for liquid and gas phases, respectively.

In this study, the diffusion phenomenon occurs in the dilute solution and is featured that chloride ion enters the static droplet. Thus,

$$k_x = \frac{CD_l}{Z} \tag{39}$$

$$k_y = \frac{pD_g}{ZRT} \tag{40}$$

where Z is the mass transfer distance [m]; R is the molar gas constant and equals to 8.314 J/(mol·K); C is the fraction of chloride ion in the liquid phase [mol/L].

HCl is dissolved in the condensation water in the form of ions and transfers at rate N, until a phase equilibrium is reached. Assume that the BFG gas-liquid mass transfer is a steady diffusion process and the droplet is hemispherical, as shown in Fig. 3, then

$$N_t = 2\pi r_0^2 N \tag{41}$$

where N_t is the total mass diffusion entering the hemispherical droplet, and r_0 is the radius of the droplet [mm].

(4) Concentration of HCl in the condensation water

As a strong electrolyte, HCl absorption in water is a dissociation equilibrium process under the following equation set:

$$\begin{cases} H_2O\,(g) \Leftrightarrow H_2O\,(l) \\ HCl\,(g) \Leftrightarrow HCl\,(aq) \\ HCl \Leftrightarrow H^+ + Cl^- \end{cases} \tag{42}$$

At the beginning of the mass transfer, the molar fractions of HCl and H_2O in the gaseous phase are y_{HCl} and y_{H_2O}, respectively; while those in the liquid phase are both 0, i.e., $x_{HCl} = x_{H_2O} = 0$.

The phase equilibrium equations are

$$x_e = \frac{y_{HCl}}{m} \tag{43}$$

and

$$y_e = m x_{HCl} \tag{44}$$

Since HCl is a strong electrolyte, its Henry coefficient (H) equals to p^0_{HCl}. In addition,

$$p_{HCl} = p \cdot y_{HCl} \tag{45}$$

According to Henry's law, we have

$$H = p_{HCl} / x_{HCl} \tag{46}$$

Then the mass fraction of HCl (w_{HCl}) in the droplet is

$$w_{HCl} = \frac{x_{HCl} \cdot M_{HCl}}{\sum_{i=1}^{2} x_i M_i} \tag{47}$$

The mass of HCl (m_{HCl}) contained in the droplet at the phase equilibrium state is

$$m_{HCl} = w_{HCl} \cdot m_{H_2O} \tag{48}$$

The amount of substance of HCl (n_{HCl}) in the droplet at the equilibrium temperature is

$$n_{HCl} = \frac{m_{HCl}}{M_{HCl}} \tag{49}$$

Thus, the amount of substance of the chloride ion (n_{Cl}) in the condensation water is

$$n_{Cl} = n_{HCl} \frac{V_{condensation\ water}}{V_{droplet}} \tag{50}$$

where $V_{condensatino\ water}$ and $V_{droplet}$ are the volumes of the condensation water and droplet, respectively. Accordingly, the concentration of the chloride ion (c_{Cl}) in the condensation water is

$$c_{Cl} = \frac{n_{Cl}}{V_{condensation\ water}} \tag{51}$$

3. Experiment

The temperature of the BFG has a double impact on the corrosion of pipelines. For one thing, the BFG temperature may influence the amount of the condensation water and the chloride ion content. For another, the temperature of BFG influences the corrosion environment. A higher BFG temperature makes pipelines easier to be corroded if condensation water already exists.

An experiment was carried out to study the corrosion phenomenon. As it is tough to simulate the change of natural environment artificially, accelerated corrosion test methods were used to shorten the experiment period. Specifically, a cyclic wet/dry exposure method was employed, which alternately put metal samples in a liquid corrosive solution and the air. Pacheco and Ferreira [33], Mansfeld and Kenkel [34] and Lyon et al. [35] pointed out that the experiment result of a cyclic exposure test agrees well with the real corrosion effect of a hanging film for a year and even longer.

3.1 Preparation of Test Pieces

The most widely used steel grade in the BFG pipelines, Q235, was selected to prepare the test pieces. The experimental material was a normalised Q235 steel plate with the size of 1000 mm × 600 mm × 4 mm.

In order to ensure the validity of the experiment, a chemical component analysis was conducted before the material is used. As shown in Fig. 4, four samples with the size of 30 mm × 30 mm at the middle of the central line and the outer line of the steel plate were sampled and sanded with an abrasive paper #120. The samples were analysed by using a Q4 TASMAN spectrometer (Bruker Elemental GmbH, Germany). The results are listed in Table 2.

A wire electrical discharge machining was used to cut the Q235 steel plate into several test pieces with a size of 50 mm × 30 mm × 4 mm. In order to eliminate the thermal effect of wire cutting on the test pieces, the test pieces were burnished by using a hand-held polisher, sanded with waterproof abrasive paper, and encapsulated with epoxy resin except for a corrosion surface. Then, the test pieces were washed by flowing distilled water and acetone and dried in a loft drier to clean the experimental surface.

3.2 Experimental Procedures

The experiment was conducted in the following sequence:

(1) The prepared test pieces were divided into five groups with three in each group, and each piece was

Table 2. *Chemical composition of the tested steel (wt.%)*

Sample no.	C	Si	Mn	S	P
1	0.146	0.228	0.475	0.025	0.023
2	0.149	0.231	0.474	0.026	0.024
3	0.146	0.226	0.47	0.025	0.019
4	0.147	0.228	0.473	0.025	0.022

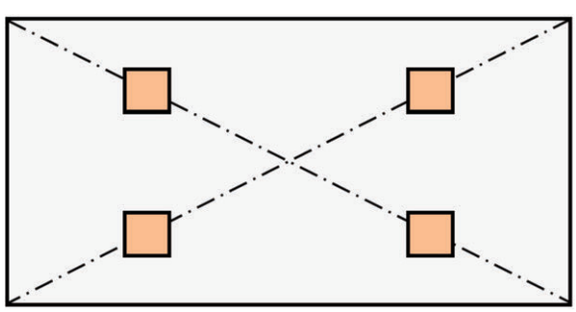

Figure 4. *The sampling locations of Q235 steel plate*

numbered and weighed.

(2) The corrosive solution was prepared as shown in Table 3 with a pure chemical reagent and distilled water.

(3) The test pieces were immersed into beakers containing the corrosive solution and were put in a thermostat at specific temperatures setting as Table 3.

(4) The test pieces were taken out after 2 h and surface-treated by a solution mixed by 500 mL hydrochloric acid, 500 mL distilled water and 3.5 g hexamethylenetetramine. Afterwards, the test pieces were washed with distilled water and acetone three times in one turn.

(5) The washed test pieces were dried in the thermostat for 2 h.

(6) Repeat steps (3) to (5) until the total time reaches 240 h.

(7) The test pieces were placed in a loft drier for 24 h. Afterwards, they were gotten out, and their appearances were observed.

(8) The corrosion products were removed for further observation. The detailed processes are as follows. A mild mechanical cleaning in the clean flowing water using a fluffy brush was needed to remove the loose corrosion products attached at the surface of these test pieces. Then, the deep-set corrosion products were removed by chemical removal, which is the same as stated in step (4).

(9) The masses of these test pieces were weighed with the accuracy of 0.1 mg, and the dimensions of the test pieces were measured with the accuracy of 0.02 mm.

(10) The corrosion morphology was observed by using a stereomicroscope and a metallographic microscope, and the pit depths were recorded.

(11) The corrosion rate and the pit depth were calculated by

$$V = \frac{(W_0 - W_1)}{S \cdot \tau} \tag{52}$$

and

$$B = \frac{8.76V}{\rho_{Q235}} \tag{53}$$

where V is the corrosion rate [g/(mm^2·h)]; W_0 and W_1 are the masses of a test piece before and after the corrosion experiment, respectively [g]; S is the area of the test piece [mm^2]; τ is the experiment time [h]; B is the pit depth [mm/a]; and ρ_{Q235} is the density of Q235 [g/cm^3].

Table 3. *Experiment groups*

Test no.	Chloride ion concentration [mol/L]	pH	Temperature [°C]
1	0.01	4	60
2	0.045	4	50
3	0.1	4	40
4	0.17	4	30
5	0.26	4	20

4. Results and Discussions

4.1 Effect of Ambient Temperature

The data of a steel plant located in Tangshan, China, were used to quantificationally analyse the mechanism of chlorine corrosion of BFG pipelines. The flow rate of BFG at the outlet of TRT unit was 500,000 m^3/h, with a temperature of 70 °C, a pressure of 12.5 kPa, a moisture content of 40 g/m^3, a chloride ion content of 22 mg/m^3 and a density of 1.3 kg/m^3. The material of the BFG pipelines was Q235-B. A 100-m long pipe was selected, whose external diameter was 4.52 m. The wall thickness was 16 mm. The pipelines were covered by an aluminium rock wool product as the thermal insulator with the thickness of 50 mm and a galvanised iron sheet plus a high-density grid glass cloth as a protective layer with the thickness of 0.5 mm.

According to Eqs. (3) and (4), the partial pressure of saturated vapour water at the outlet of TRT unit is 7405.4 Pa. The corresponding dew point temperature of pure water is 40 °C. However, the existence of chloride ion raises it to as high as 60 °C [36]. From Eq. (26), the relationship between the required time for single-phase heat transfer of the BFG, and the ambient temperature is shown in Fig. 5. It can be seen that the time of BFG single-phase convective heat transfer increases with increasing ambient temperature. The higher the ambient temperature is, the larger the increment rate of single-phase heat transfer time is. When the ambient temperature is lower than 20 °C, the increment rate of single-phase heat transfer time is 0.11 s/°C. When the ambient temperature is above 20 °C, the increment rate of single-phase heat transfer time goes up to 0.43 s/°C. This phenomenon can be approved by the convective heat transfer rate, which decreases as the heat transfer temperature difference reduces. The higher the ambient temperature is, the smaller the heat transfer temperature difference is.

The temperature of BFG at the pipe outlet also varies with the ambient temperature, as shown in Fig. 6. The BFG at the outlet of the pipeline reaches a higher temperature if the ambient temperature increases. When the ambient temperature increases from -10°C to 30°C, the overall increment rate of BFG temperature at the pipe outlet was 10.58%. This is because a higher ambient temperature will lead to a smaller condensation heat transfer amount, which also results in a higher BFG temperature at the outlet of the pipeline.

Compared with BFG temperature, the amount of chloride ion dissolved in the condensation water has an opposite effect in respect to the ambient temperature as shown in Fig. 7. As the ambient temperature increases, the concentration of chloride ion decreases. When the ambient temperature rises from -10°C to 30°C, the concentration of chloride ion varies from 0.028 mol/L to 0.005 mol/L, with an

overall descend rate of 83.30%. When the ambient temperature increases, the temperature of BFG in the pipelines increases, which leads to a longer single-phase heat transfer section. Thus, the amount of chloride ion dissolved in the condensation water is reduced significantly.

4.2 Effect of BFG Temperature

The radius of the initial condensed droplet in the BFG pipelines is set as 3 mm (see Fig. 3). The molar fraction of HCl was y_{HCl} = 0.001 when the mass transfer began. The relationship between chloride ion mass transfer rate in the liquid phase and the BFG temperature is shown in Fig. 8. It can be found that the mass transfer rate of the chloride ion increases with the increase in the BFG temperature. As it is not easy to acquire the effect of the BFG temperature on pitting corrosion theoretically, the comprehensively further analysis of the effect of BFG temperature is obtained by using the cyclic exposure test.

A stereoscopic microscope and a metallographic microscope were used to assess the corrosion effect by measuring the size, depth, and the number of corrosion pits, as shown in Fig. 9. The relationship between BFG temperature and corrosivity is extracted from the results. It is concluded that the size, depth and number of corrosion pits all increase along with the increase in the BFG temperature. When the BFG temperature reduces from 60 °C to 20 °C, the mass loss decreases from 1.13 g to 0.26 g, which further leads to a reduction of 77% in the corrsiion rate.

Fig. 10 shows the relationship between the mass loss of test pieces and the corrosion time. At the initial stage of the accelerated corrosion test (0-96 h), the mass losses of five test pieces were roughly the same. In this period, the corrosion pits of all pieces were in the state of nucleation, initiation, and growth. Temperature and chloride ion concentration were found to have a negligible effect on the corrosion phenomenon. At the mid-stage of the test, the five pieces showed different mass loss trends. The

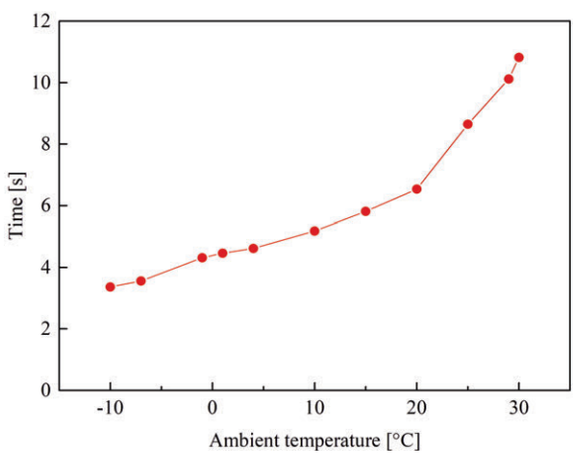

Figure 5. *BFG single-phase heat transfer time vs. ambient temperature*

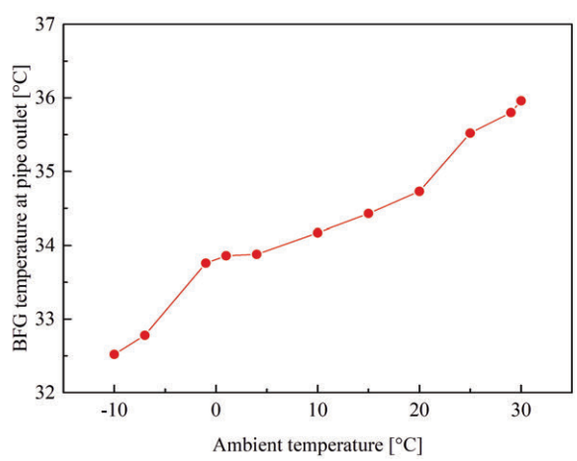

Figure 6. *BFG temperature at pipe outlet vs. ambient temperature*

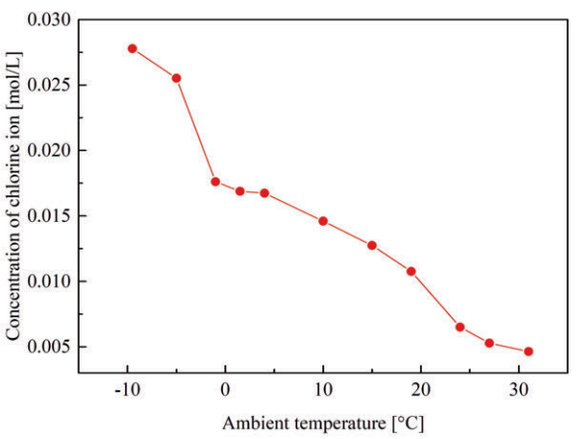

Figure 7. *Concentration of the chloride ion in the condensation water vs. ambient temperature*

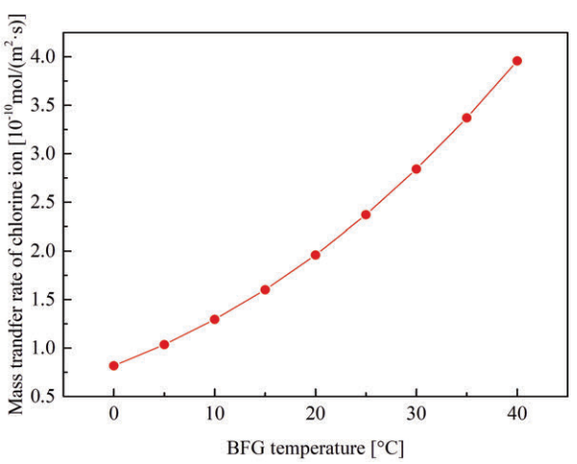

Figure 8. *Chloride ion mass transfer* rate vs. *BFG temperature*

corrosion rate of test No. 1 was faster than those of test No. 2-5 during 96-111 h, whereas, corrosion rates of test No. 4 and 5 during 144-192 h were still slow except pieces 1-3 which grew relatively fast. It indicates that BFG with higher temperature accelerates the corrosion process, while low-temperature BFG does not during this period. At the last stage of the test (192-240 h), each piece had a remarkable mass loss rate. During this stage, the corrosion pits shaped, and the pitting corrosion shifted towards the rapid growth period, resulting in a larger corrosion rate.

4.3 Conceptual Anticorrosion Design by Using Process Heat

The precipitation of condensation water and chloride ion in BFG pipelines is a continuous process accompanied by the blast furnace iron-making, which corrodes the BFG pipelines. However, no condensation water would be precipitated if the BFG temperature is higher than its dew point. Under this condition, it is impossible for the chloride ions to be dissolved in the condensation water to become the corrosive liquid. Therefore, a conceptual design of anticorrosion is proposed by increasing the BFG temperature to prevent the pipelines from being corroded.

In the conceptual anticorrosion design, the BFG pipeline after the TRT unit is covered by an additional tube. The low-pressure hot fluid passes through the tube and heats up the BFG to a temperature higher than the dew point, as shown in Fig. 11. Given that the whole pipeline network is complex and long-distance, it is difficult to maintain the BFG temperature always above the dew point unless using hot fluids to warm the whole BFG pipeline network. Therefore, the

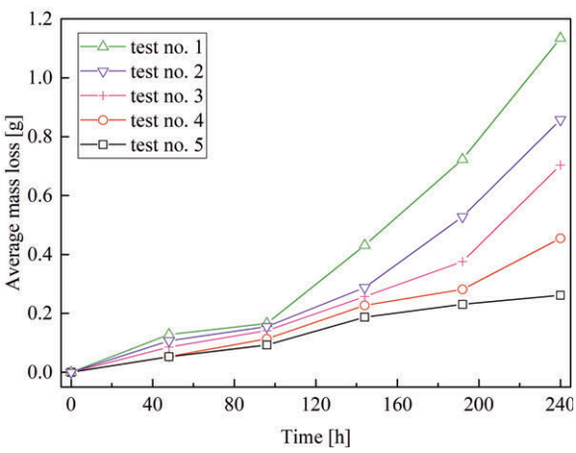

Figure 10. *Average mass loss profile with time*

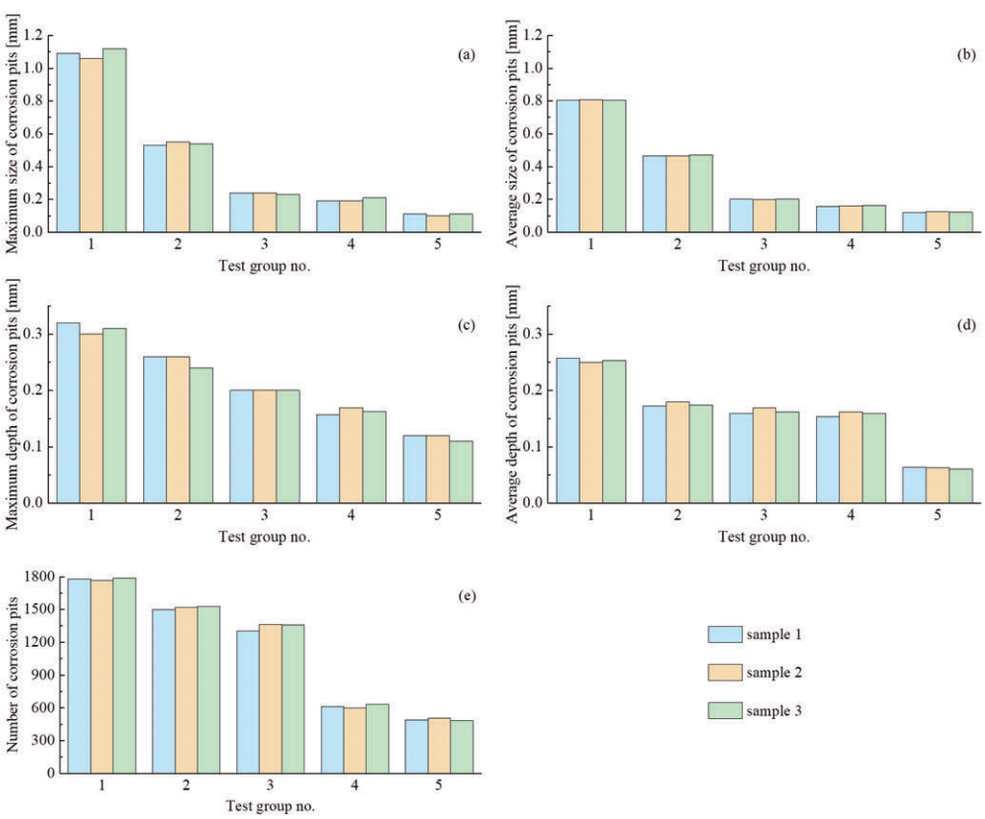

Figure 9. *Statistical corrosion pits data of the cyclic exposure test. (a) Maximum size; (b) Average size; (c) Maximum depth; (d) Average depth; and (e) Density*

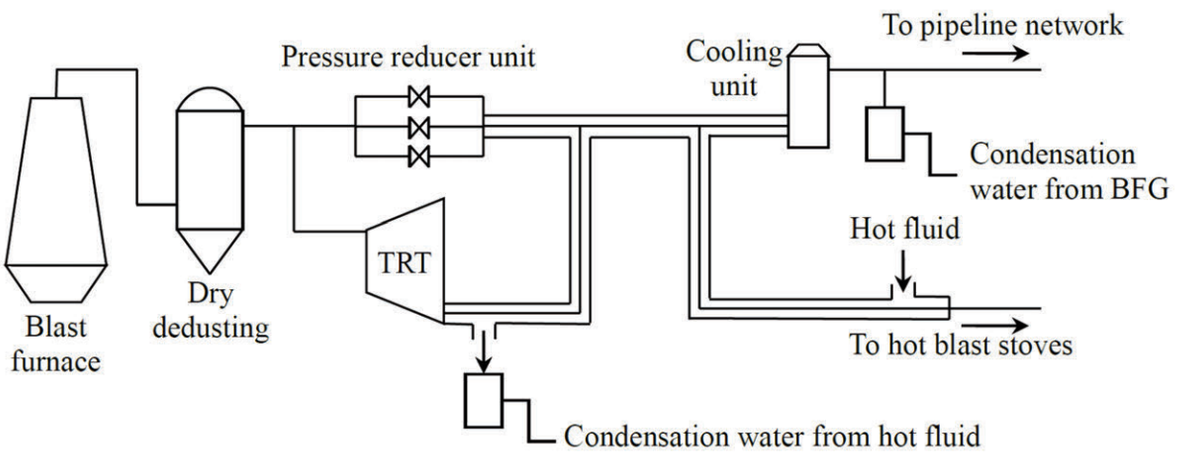

Figure 11. *Schematic diagram of the conceptual anticorrosion design*

pipelines between the TRT unit and the hot blast stoves are suggested to be covered by the additional tube due to its relatively short distance. The heated BFG increases the thermal efficiency of the hot blast stoves. The BFG transported through long distance is rapidly cooled to separate the corrosive chloride ion and condensation water. By combining these two methods, the whole BFG pipeline network is prevented from being corroded.

5. Conclusion

(1) Thermal models were established to explore the chlorine corrosion process from a thermal perspective. The models can calculate the amount of condensation water from the BFG under different ambient temperature, the mass transfer rules of chloride ion, and the concentration of chloride ion in condensation water. When the ambient temperature rose from -10 °C to 30 °C, the concentration of chloride ion was reduced by 83.30%.

(2) A cyclic exposure experiment was conducted, with Q235, to investigate the co-effect of BFG temperature and chloride ion concentration on the corrosion. It was shown that the corrosion rate of test pieces declined as the BFG temperature was reduced. When the BFG temperature was reduced from 60 °C to 20 °C, the corrosion rate was also reduced by 77%.

(3) A conceptual anticorrosion design was proposed based on the models and experimental results. This design integrates a tube and a cooling unit into the BFG pipeline, which prevents the BFG pipeline from being corroded without using new additional materials. However, further studies are needed on this topic.

Acknowledgement

This work was supported by the National Natural Science Foundation of China (51704069), and the China State Scholarship Fund – International Clean Energy Talent Program (CSC-iCET-201802180028).

References

[1] Clarke Energy, https://www.clarke-energy.com/steel-production-gas/.

[2] W. Sun, Y. Wang, F. Zhang, Y. Zhao, Eng. Opt., 50 (9) (2018) 1578-1592.

[3] C.H. Li, J.L. Zhang, C. Wang, B.J. Yan, Y.P. Zhang, H.W. Guo, in Characterization of Minerals, Metals, and Materials 2017 (S. Ikhmayies, B. Li, J.S. Carpenter, J. Li, J.Y. Hwang, S.N. Monteiro, D. Firrao, M. Zhang, Z. Peng, J.P. Escobedo-Diaz, C. Bai, Y.E. Kalay, R. Goswami, J. Kim), Springer International Publishing, Gewerbestrasse, 2017, pp. 737-746.

[4] Z. Lei, W. Zhu, Metall. Power, 1 (2011) 22-23.

[5] X. Li, W. Sun, L. Zhao, J. Cai, Environ. Technol., 40 (3) (2019) 282-292.

[6] A. Lajtonyi, Millennium Steel, (2006) 57-75.

[7] W. Sun, X. Yue, Y. Wang, Energy Convers. Manag., 135 (2017) 63-73.

[8] W. Sun, X. Yue, Y. Wang, J. Cai, J. Central South Univ., 25 (6) (2018) 1464-1474.

[9] Q. Wang, L.J. Wang, Y.Q. Liu, K.C. Chou, J. Min. Metall. Sect. B-Metall., 53 (3) B (2017) 365-372.

[10] D. Ashkenazi, A. Inberg, D. Cvikel, J. Min. Metall. Sect. B-Metall., 54 (1) B (2018) 101-110.

[11] R. Nyborg, Business Brief. Explor. Product. Oil Gas Rev., 2 (2005) 70-74.

[12] J.L. Zhang, C. Wang, H.B. Zuo, K.X. Jiao, Z.Y. Wang, Iron Steel, 7 (2015) 1-7.

[13] M. Palcut, L. Ďuriška, M. Špoták, M. Vrbovský, Ž. Gerhátová, I. Černičková, J. Janovec. J. Min. Metall. Sect. B-Metall., 53 (3) B (2017) 333-340.

[14] M. Geerdes, R. Chaigneau, I. Kurunov, O. Lingiardi, J. Ricketts, Modern Blast Furnace Ironmaking: An Introduction, third ed., IOP Press, Amsterdam, 2015.

[15] B.S. Hu, Y.L. Gui, K. Lü, J.J. Mi, J. Iron Steel Res., 1 (2013) 23-25.

[16] I.V. Murav'eva, G.I. Bebeshko, Steel Translation, 47 (2017) 287-290.

[17] H. Bartusch, T. Hauck, H.G. Grabietz, Stahl und Eisen, 134 (2014) 51-56.

[18] B.S. Hu, Y.L. Gui, H.L. Guo, C.Y. Song, Adv. Mater. Res., 396-398 (2012) 152-156.

[19] X.L. Hu, H.L. Li, L. He, Shandong Metall., 28 (6) (2006) 52-53 (in Chinese).

[20] Z.Y. Gao, L.P. Liang, Z.Q. Liu, Metall. Power, 4 (2008) 28-29 (in Chinese).

[21] Y. Zeng, K. Li, R. Hughes, J.L. Luo, Indus. Eng. Chem. Res., 56 (48) (2017) 14141-14154.

[22] S.C. Okoro, M. Montgomery, F.J. Frandsen, K. Pantleon, Energy Fuels, 32 (7) (2018) 7991-7999.

[23] C.A. Sleicher, M.W. Rouse, Int. J. Heat Mass Transfer, 18 (5) (1975) 677-683.

[24] I. Kotcioglu, M.N. Khalaji, A. Cansiz, Appl. Therm. Eng., 132 (2018) 637-650.

[25] J.B. Chaddock, Refrig. Eng., 65 (4) (1957) 36-41.

[26] S.C. Chato, ASHRAE J., 4 (2) (1962) 52-60.

[27] S.W. Churchill, H.H.S. Chu, Int. J. Heat Mass Transfer, 18 (9) (1975) 1049-1053.

[28] W.G. Whitman, Chem. Metall. Eng., 29 (4) (1923) 146-148.

[29] L.P. Burkhard, A.W. Andren, D.E. Armstrong, Environ. Sci. Technol., 19 (6) (1985) 500-507.

[30] R.B. Bird, W.E. Stewart, E.N. Lightfoot, Transport Phenomena, John Wiley, New York, 1960.

[31] S.W. Shin, H.C. No, Nuclear Technol., 73 (3) (1986).

[32] E. Alpay, M. Demircioğlu, Mass Transfer and Mass Transfer Operations, Ege Univ., İzmir, 2006, pp. 68-72.

[33] A.M.G. Pacheco, M.G.S. Ferreira, Corrosion Sci., 36 (5) (1994) 797-813.

[34] F. Mansfeld, J.V. Kenkel, Corrosion Sci., 16 (3), (1976) 111-122.

[35] S.B. Lyon, G.E. Thompson, J.E. Johnson, G.C. Wood, J.M. Ferguson, Corrosion, 45 (1989) 951-957.

[36] H. Pan, Energy Conserv., 1 (2016) 67-69 (in Chinese).

HLORSKA KOROZIJA CEVI ZA VISOKOPEĆNI GAS: ANALIZA IZ TERMALNE PERSPEKTIVE

W.-Q. Sun [a,b,c*], X.-D. Xu [b], Y. Zhang [d], J.-Z. Wu [b]

[a] Odsek za termalno inženjerstvo, Fakultet za metalurgiju, Severnoistočni univerzitet, Šenjang, Lijaoning, Kina

[b] Fakultet za inženjerstvo, Univerzitet u Kardifu, Vels, Ujedinjeno Kraljevstvo

[c] Glavna državna laboratorija eko-industrije za zaštitu okoline, Šenjang, Lijaoning, Kina

[d] R&D centar, Hisense Grupa Co., Ltd., Ćingdao, Šandong, Kina

Apstrakt

Zajedno sa širokom primenom suvog otpraš̆ivanja visokopeœnog gasa (BFG), pojavljuje se i problem korozija cevi za visokopeœni gas zbog hlora koji se nalazi u BFG. Postojeœe metode za spreèavanje korozije kao što su prskanje bazama ili ugradnja materijala otpornih na koroziju zahtevaju znatna ulaganja. U ovom radu izvedena je originalna termalna analiza mehanizma korozije da bi se podržala studija o spreèavanju korozije bez koriš̆œenja dodatnih materijala. Najpre su ustanovljeni modeli koji odražavaju odnos između koliène kondenzovane vode, brzine prenosa mase, koncentracije hloridnog jona i temperature okoline. Zatim je uz pomoœ eksperimenta cikliènog izlaganja dobijen odnos između BFG temperature i brzine korozije. Identifikovani su ključni faktori koji utièu na koroziju cevi pod uslovima razlièitih BFG temperatura. Konaèno, predložena je kontrolna šema BFG temperature da bi se izbegla hlorska korozija.

***Ključne reči**: Hlorska korozija; Cevi za visokopećni gas; Suvo otpraš̆ivanje; Termalna analiza; Test cikličnog izlaganja.*